Final Report of Semiconductor Photonic Devices Design

Mike Mai
Affiliation not available

***Abstract*—The purpose of this report is to design, fabricate and test a group of TE silicon photonics devices using Klayout, Lumerical Interconnect and measurement analysis. The report is also going to introduce some basic design concept of a photonic device, an is going to observe the effect of different waveguide parameters on the performance of the device. An indirect relationship between refractive index (either group or effective) and wavelength is going to be developed in this report. Later on, we are going to compare the result from simulation with the measurement result by plotting the same transmission curve and extracting device parameters from measurement data.**

INTRODUCTION

Over the centuries, silicon has become the most ubiquitous material in the electronic industry. Particularly, silicon-on-insulator (SOI) wafer becomes the most ideal platform for creating planar photonics device because of its strong optical confinement offered by the high index contrast between silicon (n=3.45) and SiO_2 (n=1.45) [1]. It is possible to scale photonic devices to hundreds of nanometer level; therefore silicon has chosen to be the top material choice for massive production of optical devices.

On the other hand, Bragg grating waveguide is a photonic device, contained of arrays of partially overlapped refractive index voxels [2]. These refractive index voxels create a one-dimensional photonic bandgap, which allows only a narrow spectrum of a broadband signal to be reflected and propagated through the waveguide. With this unique characteristics, Bragg grating waveguide can simultaneously produce a low light-loss output and have a high grating resonance.

In this report, we are going to investigate the interaction between silicon and Bragg grating wavegudie, and analyze the performance of this particular photonic device. The report is going to first introduce the theory and the design concept behind each device. A detailed simulation result and analysis are also included to observe the effect of different design parameters on the quality factor of each device. We are also going to provide a thoughtful comparison between the simulated result and the measured result after the photonics ship get fabricated at two foundries: Applied Nanotools Inc. and Washington Nanofabrication Facility. We are also going to extract circuit parameters such as the effective refractive index and free spectra range from the measurement data, and best curve fit the measured raw data to gain a better insight into the performance of each designed photonic devices.

TECHNOLOGY AND THEORY

Mathmatically, quality factor (Q) measures the ratio between energy stored and energy lost per cycle. It can also defined as $Q = \omega \cdot \tau_p = 2\pi \frac{c}{\lambda} \frac{n_g}{c} \frac{1}{\alpha} = 2\pi \frac{n_g}{\lambda \alpha}$ (1)

where $\tau_p = \frac{n_g}{c\alpha}$, α is the total power loss and mirror loss, ω is the angular frequency, and n_g is the group effective index.

According to the equation defined above, the theoretical maximum quality factor is at the maximum, $2\pi n_g$, when the denominator $\lambda \cdot \alpha$ is equal to 1. In real world, it is impossible to have no energy loss, but we can assume that there is no mirror loss by having a infinite long Bragg mirror. In this case, we can find α as the total power loss in m^{-1} thus finding the "maximum"theoretical possible quality factor. However, we need to finite Bragg grating in order to have light coming in and out and be able to measure it. At the end, the quality factor is usually lower than the theoretical maximum value [3].

For any types of Bragg reflectors, the reflected wavelength, λ_B , is defined by the Bragg condition, $\lambda_B = 2n_{eff}\Lambda$, where n_{eff} is the effective refractive index of the wavegudie and Λ is the grating period. With this relationship, we should limit the grating period and effective refractive index in order to obtain a high quality factor, since quality factor is inversely proportional to the reflected wavelength.

Besides that, the period between the peaks of the MZI transfer function, the free spectral range is defined as $FSR(\lambda) = \frac{\lambda^2}{\Delta L \cdot n_g(\lambda)}$,

where $n_g\ (\lambda) = n_{eff}(\lambda) - \lambda \cdot \frac{dn_{eff}}{d\lambda}$

MODELING AND DESIGN METHODOLOGY

In this report, the primary software used for modeling and simulation were Lumerical Interconnect and Klayout. Transfer Matrix Method was expected to be performed before masking the layout as it can help us obtaining the three coefficients of the waveguide compact model and a desired TMM spectrum. We were also expected to investigate into the relationship between the wavelength and the waveguide effective refractive index while developing our model so that we can obtain a quality factor as high as possible. However, due to some extreme circumstances and time constraint, we were not able to construct a physical structure matrix and an ideal transfer function with Transfer Matrix Method and MATLAB during the design phase. That being said, the models that we designed were not based on any compact model equation or transfer function, but rather based on experimental db-gain plot. The simulated result might not be as accurate as we expected.

The model shown in Figure 3 was our first design. By varying the waveguide path length and adding a taper component to our first design, we concluded that the total gain of the device is dependent on the waveguide path length and taper affects the

number of peaks that a device can have. As we increased the waveguide length, the number of peaks increases. By adding a Taper to the device, the transmission signal got filtered and less noise were observed. The number of peaks also decreased, but the magnitude of each peak increased when we included a Taper in our design. We also tried to alter the parameters of the waveguide in each design to observe the effect of different waveguide radius or waveguide widths.

As shown in Figure 1, the TE device model comprises several key components: a) Grating Couplers to couple light between thin-film waveguides and a single-mode fiber [4]. b) TE Bragg Grating to reflect specific wavelengths of light and transmits all others. c) TE Tapers to improve coupling to small-area waveguides and guiding to high-orders guided modes (Mode Matching and Mode Filtering) [5]. d) Waveguide for light or electromagnetic waves to channel through space.

The upper grating coupler is treated as the laser where light gets injected, and the bottom grating coupler is the detector. Figure 2 is the circuit schema of the layout shown in 1 in Lumerical Interconnect.

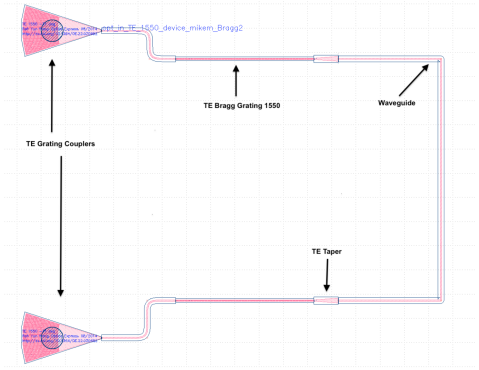

Figure 1. Structure Layout of a simple TE Photonic Device

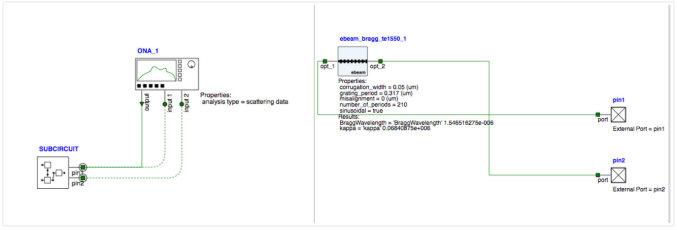

Figure 2. Circuit Schema in Lumerical Interconnect

SIMULATION

Figure 3 to Figure 8 are a list of Bragg grating waveguide designs for fabrication and later on analysis. Each figure consists a design layout and its corresponding TE gain plot, transmission plot and Free Spectral Range(FSR) plot. Each of the TE gain plots also highlight the estimate location of the TE quality factor. Figure 9 is the TE compact model of the design where light is injected at the upper TE grating coupler (lasing) and Figure 10 is the TE compact model where light is injected at Port 1 at mode 1. Figure 11 consists both a)Effective Refractive Index vs. Wavelength and b)Group Effective Index vs. Wavelength plots. In Appendix A, Table I shows simulated result and parameters from each design; whereas Table II shows the variation in waveguide between each design. For all layouts, the grating period is 0.317 μm and corrugation width is 0.05 μm.

As shown in Figure 11, there is an indirect relationship between the Bragg grating wavelength and the effective indices of the waveguide. To be clear, the effective refractive index n_{eff} tends to decrease as the wavelength increases. The group effective index n_g increases as the wavelength increases.

The effect of different waveguide length are depicted in Figure 4 and Figure 7 for path difference of 110.29 μm for the fundamental quasi-TE mode. In the case when the waveguide length increases, the number of peaks increases and the free spectral range (FSR) also seems to shift slightly to the right. The quality factor of design 4 was 1.5 times amplified compared to the quality factor of design 7. As shown in Figure 5 and Figure 6, the number of peaks and the magnitude of the quality factor are increased dramatically as we increase both of the waveguide radius and waveguide length. The range of FSR also extends as well. This observation reinforces our previous notion where an increase in waveguide path increases the number of peaks and the magnitude of the quality factor. In addition, if we increase the waveguide width and decrease the waveguide radius while having same waveguide path length, the number of peaks and the magnitude of the quality factor remain the same. This conclusion is shown in Figure 3 and Figure 7.

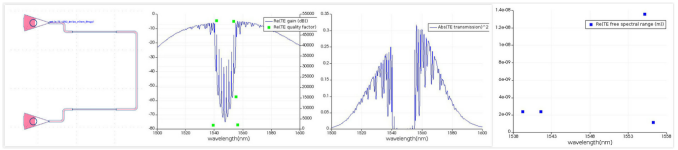

Figure 3. TE Bragg Grating Design 1 (Design Layout, Gain & Quality Factor Plot, Transmission Plot)

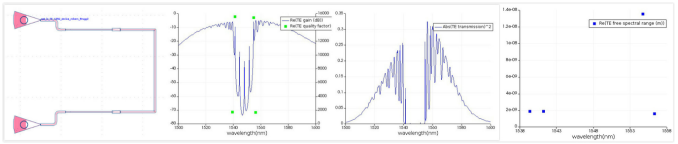

Figure 4. TE Bragg Grating Design 2 (Design Layout, Gain & Quality Factor Plot, Transmission Plot)

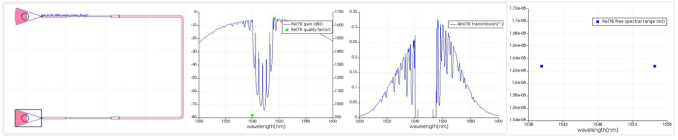

Figure 5. TE Bragg Grating Design 3 (Design Layout, Gain & Quality Factor Plot, Transmission Plot)

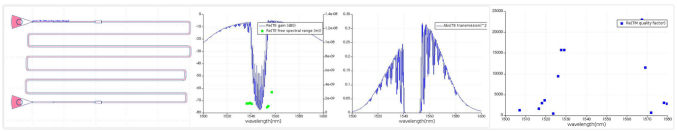

Figure 6. TE Bragg Grating Design 4 (Design Layout, Gain & Quality Factor Plot, Transmission Plot)

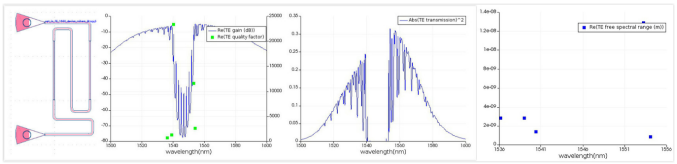

Figure 7. TE Bragg Grating Design 5 (Design Layout, b)Gain & Quality Factor Plot, Transmission Plot)

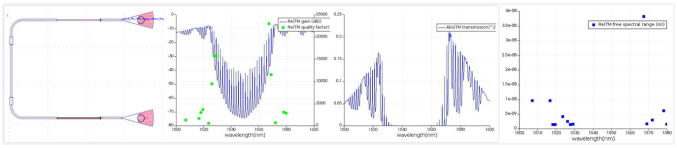

Figure 8. TM Bragg Grating Design (Design Layout, Gain & Quality Factor Plot, Transmission Plot)

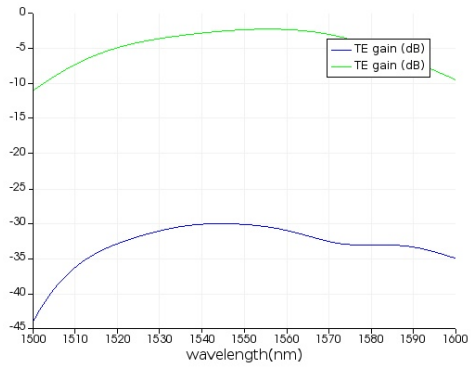

Figure 9. TE Mode Compact Model, light injected at TE 1550 grating coupler

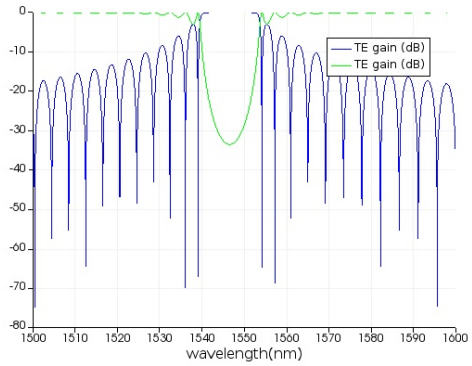

Figure 10. TE Mode Compact Model, light injected at Port 1

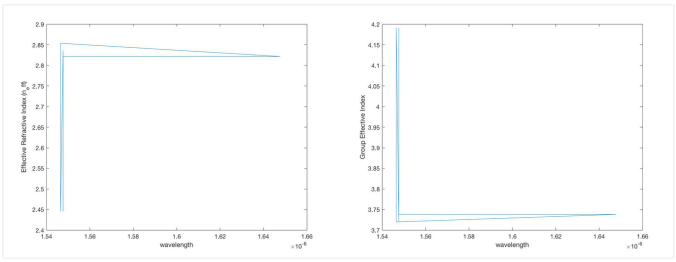

Figure 11. a) Effective Refractive Index vs. Wavelength b) Group Effective Index vs. Wavelength

I. Fabrication

The Bragg grating waveguides that we analyze in this report were fabricated on two chips at two separate foundries: Applied Nanotools Inc. and Washington Nanofabrication Facility. These two manufacturers apply different fabrication technique and process. For instance, Applied Nanotools Inc. uses the NanoSOI MPW fabrication process and Washington Nanofabrication Facility uses the silicon Photonic process.

The NanoSOI MPW fabrication process used by Applied Nanotools Inc. is based on direct-write 100 keV electron beam lithography technology [0]. This process has the advantages of rapid prototyping while having the capability to produce a device with high optical performance and low propagation loss. Silicon-on-insulator wafers of 200 mm diameter, 220 nm device thickness and 2μm buffer oxide are used as the base material for the fabrication. The wafer was pre-diced into square substrates with dimensions of 25x25 mm, and lines were scribed into the substrate backsides to facilitate easy separation into smaller chips once fabrication was complete. After an initial wafer clean using piranha solution of 3:1 H_2SO_4 and H_2O_2 for 15 minutes, the wafer got rinsed thoroughly by either water or Isopropyl Alcohol (IPA). A Hydrogen Silsesquioxane (HSQ) resist was then spin-coated onto the substrate and got heated to evaporate the solvent. In addition, the Photonic devices were patterned using a Raith 5000+ electron beam instrument with a raster step size of 5 nm. The exposure dosage of the design was corrected for proximity effects that result from the backscatter of electrons from exposure of nearby features. Shape writing order was optimized for efficient patterning and minimal beam drift. After the E-beam exposure and subsequent development with a Tetramethylammonium hydroxide (TMAH) solution, the devices were inspected optically for any residues and defects. If no defects or errors were reported, the devices were then ready for next etching procedure. The devices would got mounted on a 4" handle wafer and underwent an Anisotropic ICP-RIE etch process using Chlorine gas. The resist was removed from the surface of the devices using a 10:1 buffer oxide wet etch, and the devices were inspected using a scanning electron microscope (SEM) to verify patterning and etch quality. A 2.2 μm oxide cladding was deposited using a plasma-enhanced chemical vapour-deposition (PECVD) process based on Tetraethyl Orthosilicate (TEOS) at 300 °C. Reflectometry measurements were performed throughout the process to verify the device layer, buffer oxide and cladding thicknesses before delivery.

On the other hand, Washington Nanofabrication Facility

fabricates the Phontonics devices using the Silicon Photonics process [0]. This process is also based on 100 keV electron beam lithography, but silicon-on-insulator wafers of 150 mm diameter, 220 nm thick silicon and 3 μm silicon dioxide thickness were used as the base material. The wafer was also pre-diced into square substrates with 25x25 mm. After a solvent rinse and hot-plate dehydration bake, HSQ was spin-coated at 4000 rpm and got heated at 80 °C for 4 minutes. Electron beam lithography was performed using a JEOL JBX-6300FS system operated at 100 keV energy, 8 nA beam current, and 500 μmexposure field size. A 1 nm machine grid was used for shape placement, and the spacing between dwell points during the shape writing was 6 nm. An exposure dose of 2800 $\frac{\mu C}{cm^2}$ was used. The resist was developed by immersion in 25 percent of TMAH for 4 minutes, followed by a flowing deionized water rinse for 60 seconds and an Isopropanol rinse for another 10 seconds. At the end, the resist got blown dry with nitrogen gas. After all of these steps, the silicon was removed from unexposed areas using inductively coupled plasma etching in An Oxfod Plasmalab System 100, with a Chlorine gas flow of 20 standard cubic centimeters per minute ($SCCM$), pressure of 12 mT, ICP power of 800 W, bias power of 40 W, a bias voltage of 185 V a constant temperature of 20 °C. During etching, chips were mounted on a mm silicon carrier wafer using Perfluoropolyether (PFPE) vacuum oil. Cladding oxide was deposited using plasma enhanced chemical vaporized deposition (PECVD) in an Oxford Plasmalab System 100 with a Silane (SiH_4) flow of 13.0 $SCCM$, Nitrous oxide (N_2O) flow of 1000.0 $SCCM$, high-purity nitrogen (N_2) flow of 500.0 $SCCM$, pressure at 1400 mT, high-frequency RF power of 120W, and a constant temperature of 350 °C. During deposition, chips rest directly on a silicon carrier wafer and are buffered by silicon pieces on all sides to promote uniformity.

II. Measurements

In order to characterize and analyze the performance of the fabricated devices, a custom-built automated test setup [0] [0] with automated control software written in Python was used [0]. An Agilent 81600B tunable laser was used as the input source and Agilent 81635A optical power sensors as the output detectors. The wavelength was swept from 1500 to 1600 nm in 10 pm steps (or 1 pm steps for those that requested it). A polarization maintaining (PM) fibre was used to maintain the polarization state of the light, to couple the TE polarization into the grating couplers [4] (or TM if you designed your circuits for TM, in which case a 90º rotation was used to inject light into the TM grating couplers [4]). A polarization maintaining fibre array was used to couple light in/out of the chip [5].

We perform measurement data analysis on the fabricated devices. Figure 12 to Figure 17 are the result from measurement. From these figure, we understand that the measured result shares similar waveform with the simulated result.

III. Acknowledgments

I acknowledge the edX UBCx Phot1x Silicon Photonics Design, Fabrication and Data Analysis course, which is supported by the Natural Sciences and Engineering Research Council of Canada (NSERC) Silicon Electronic-Photonic Integrated Circuits (SiEPIC) Program. The devices were fabricated by a) Richard Bojko at the University of Washington Washington Nanofabrication Facility, part of the National Science Foundation's National Nanotechnology Infrastructure Network (NNIN), and/or b) Cameron Horvath at Applied Nanotools, Inc. Hossam Shoman performed the measurements at The University of British Columbia. I acknowledge Lumerical Solutions, Inc., Mathworks, Python, and KLayout for the design software. I would like to greatly thank Professor. Lukas Chrostowski for his excellent teaching and guiding throughout the course.

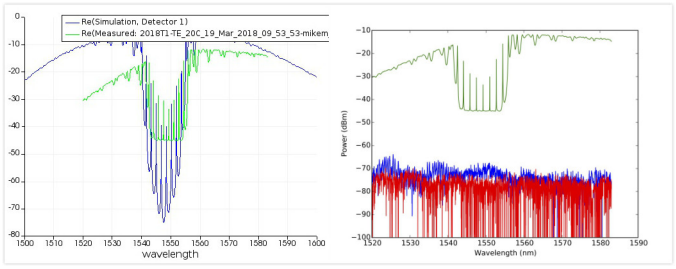

Figure 12. TE Device 1 Measurement Data vs. Simulation Data

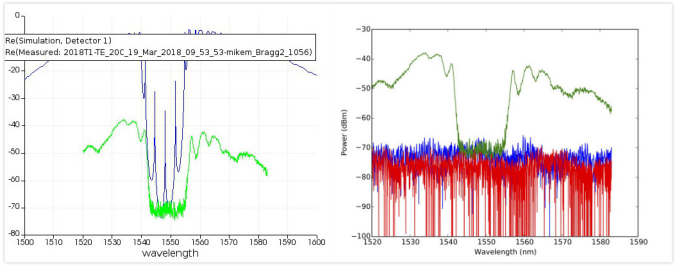

Figure 13. TE Device 2Measurement Data vs. Simulation Data

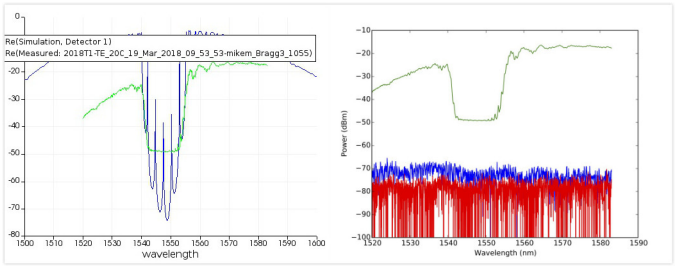

Figure 14. TE Device 3 Measurement Data vs. Simulation Data

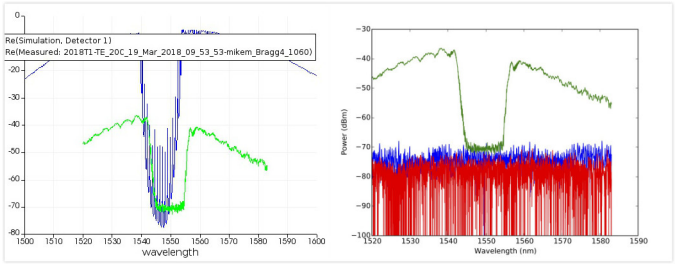

Figure 15. TE Device 4 Measurement Data vs. Simulation Data

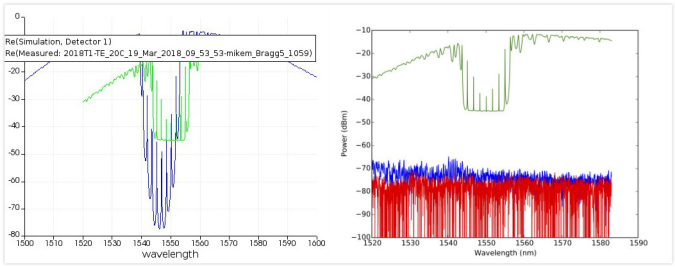

Figure 16. TE Device 5 Measurement Data vs. Simulation Data

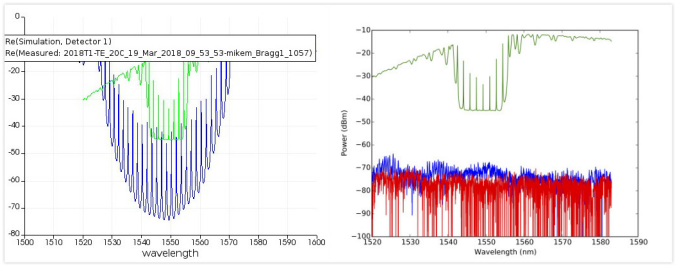

Figure 17. TM Device 1 Measurement Data vs. Simulation Data

Conclusion

Throughout the report, we provided an in-depth analysis on each Bragg grating designs, with simulation from Lumerical Interconnect and MATLAB. We observed how would different waveguide parameters affect the characteristics of each device. According to our simulation, we understood that the number of the peaks increases as we extend the waveguide path length or the waveguide radius. The magnitude of its quality factor also gets amplified as we increase the waveguide path length and waveguide parameters. As the grating wavelength increases, the group effective index also increases but the effective refractive index decreases. In comparison to the simulated result, the measured transmission plots tend to share the same waveform as the simulated transmission plots. Nevertheless, the magnitudes of the measurement data tend to be smaller than the simulation data. On the other hand, since there exists time constraints and other extreme circumstances, Transfer Matrix Method was not able to be performed before the actual layout design. The accuracy of our plots and simulation results were not as high as we expected because we did not develop a transfer function for each of our devices. For future similar experiment or study, a best curve fit for the transmission plot can be plotted to profoundly investigate the characteristics of each photonic device. A parameter extraction from the measurement result could also have been done to examine whether there exists a difference between the measured parameters and simulated parameters.

Appendix

Bragg Grating Design	Ng1	Ng2	Neff1	Neff2
TE1	4.19	4.19	2.45	2.45
TE2	4.19	3.74	2.45	2.82
TE3	4.19	3.74	2.45	2.82
TE4	4.19	3.72	2.45	2.85
TE5	4.19	4.19	2.45	2.45
TM1	4.19	3.72	2.45	2.84

Bragg Grating Design	Kappa	Q	Wavelength
TE1	75375.25	23352.5	1.55e-06
TE2	75375.25	15572	1.55e-06
TE3	75375.25	916.78	1.55e-06
TE4	68408.75	23373	1.55e-06
TE5	68408.75	23371	1.55e-06
TM1	75375.25	22970.5	1.55e-06

Table I. Simulation Result of each Bragg grating Design

Bragg Grating Design	Waveguide Width	Waveguide Radius
TE1	0.5	5
TE2	5	0.5
TE3	5	2
TE4	5	3
TE5	5	0.5
TM1	15	0.5

Table II. Waveguide Variation

REFERENCES

[1] B. Jalali and S. Fathpour, "Silicon Photonics," *Journal of Lightwave Technology*, vol. 24, no. 12, pp. 4600–4615, dec 2006. [Online]. Available: https://doi.org/10.1109%2Fjlt.2006.885782

[2] "3D Bragg Grating Waveguide Devices," https://link.springer.com/chapter/10.1007Tue, April 24, 2018. [Online]. Available: https://link.springer.com/chapter/10.1007/978-3-642-23366-1_9

[3] L. Chrostowski and M. Hochberg, *Silicon Photonics Design*. Cambridge University Press, 2015. [Online]. Available: https://doi.org/10.1017%2Fcbo9781316084168

[4] D. Taillaert, F. V. Laere, M. Ayre, W. Bogaerts, D. V. Thourhout, P. Bienstman, and R. Baets, "Grating Couplers for Coupling between Optical Fibers and Nanophotonic Waveguides," *Japanese Journal of Applied Physics*, vol. 45, no. 8A, pp. 6071–6077, aug 2006. [Online]. Available: https://doi.org/10.1143%2Fjjap.45.6071

[5] "Encyclopedia of Laser Physics and Technology - tapered fibers, supercontinuum generation," https://www.rp-photonics.com/tapered$_fibers.html, accessedonThu, April26, 2018.[Online].Available:$

"NanoSOI Fabrication Process — Applied Nanotools Inc." http://www.appliednt.com/nanosoi, accessed on Tue, April 24, 2018. [Online]. Available: http://www.appliednt.com/nanosoi

R. J. Bojko, J. Li, L. He, T. Baehr-Jones, M. Hochberg, and Y. Aida, "Electron beam lithography writing strategies for low loss high confinement silicon optical waveguides," *Journal of Vacuum Science & Technology B, Nanotechnology and Microelectronics: Materials, Processing, Measurement, and Phenomena*, vol. 29, no. 6, p. 06F309, nov 2011. [Online]. Available: https://doi.org/10.1116%2F1.3653266

L. Chrostowski and M. Hochberg, *Silicon Photonics Design*. Cambridge University Press, 2015. [Online]. Available: https://doi.org/10.1017%2Fcbo9781316084168

"Home," http://mapleleafphotonics.com, accessed on Tue, April 24, 2018. [Online]. Available: http://mapleleafphotonics.com/

"Automated Probe Station — siepic.ubc.ca," http://siepic.ubc.ca/probestation, accessed on Tue, April 24, 2018. [Online]. Available: http://siepic.ubc.ca/probestation